Solution structure of the second PDZ domain of the neuronal adaptor X11alpha and its interaction with the C-terminal peptide of the human copper chaperone for superoxide dismutase

Duquesne, A.E.; Ruijter, M. de; Brouwer, J.; Drijfhout, J.W.; Nabuurs, S.B.; Spronk, C.A.E.M.; ... ; Canters, G.W.

Article

Solution structure of the second PDZ domain of the neuronal adaptor X11α and its interaction with the C-terminal peptide of the human copper chaperone for superoxide dismutase

Aude E. Duquesne[a], Martina de Ruijter[a], Jaap Brouwer[a], Jan W. Drijfhout[b],
Sander B. Nabuurs[c], Chris A. E. M. Spronk[c], Geerten W. Vuister[d],
Marcellus Ubbink[a],* & Gerard W. Canters[a]
[a]*Leiden Institute of Chemistry, Leiden University;* [b]*Department of Immunohematology and Blood Transfusion, Leiden University Medical Center, Leiden;* [c]*CMBI, Radboud University Nijmegen;* [d]*Department of Biophysical Chemistry, Institute for Molecules and Materials, Radboud University, Nijmegen, The Netherlands*

Abstract

Protection against reactive oxygen species is provided by the copper containing enzyme superoxide dismutase 1 (SOD1). The copper chaperone CCS is responsible for copper insertion into apo-SOD1. This role is impaired by an interaction between the second PDZ domain (PDZ2α) of the neuronal adaptor protein X11α and the third domain of CCS (McLoughlin et al. (2001) *J. Biol. Chem.*, **276**, 9303–9307). The solution structure of the PDZ2α domain has been determined and the interaction with peptides derived from CCS has been explored. PDZ2α binds to the last four amino acids of the CCS protein (PAHL) with a dissociation constant of 91 ± 2 μM. Peptide variants have been used to map the interaction areas on PDZ2α for each amino acid, showing an important role for the C-terminal leucine, in line with canonical PDZ-peptide interactions.

Abbreviations: CCS – copper chaperone for SOD1; HOAc – acetic acid; PDZ – post-synaptic density 95, *Drosophila* disks-large, *Zona occludens* 1; RP-HPLC – reversed phase high-performance liquid chromatography; SOD1 – superoxide dismutase 1

Introduction

Metal chemistry plays an important role in many essential biological enzymatic reactions. As metals are highly reactive in solution, free metal ions are virtually absent in the cell (Rae et al., 1999). Metals are transported to the target enzymes by metal chaperone proteins, like the chaperone CCS for copper insertion into superoxide dismutase 1 (SOD1), which is involved in removal of reactive oxygen species (ROS) (Harrison et al., 1999; Pena et al., 1999; O'Halloran and Culotta, 2000).

CCS presumably obtains Cu(I) from one of the copper transporters at the plasma membrane and transports it to the cytoplasmic SOD1 (Culotta et al., 1997). CCS consists of three domains, numbered I, II and III from the N- to the C-terminus of the protein. CCSI binds the Cu(I), CCSII recognizes the target protein (SOD1), and CCSIII is believed to help copper delivery from CCSI into the copper site of SOD1 (Falconi et al., 1999;

*To whom correspondence should be addressed. E-mail: m.ubbink@chem.leidenuniv.nl

Rosenzweig and O'Halloran, 2000), although there is no evidence for this mechanism. Crystals of CCS allowed the determination the structures of CCSI and CCSII, but not of CCSIII, suggesting a flexible nature for that domain (Lamb et al., 1999). This flexibility is believed to be of importance for copper delivery. Indeed, CCSI and the copper site of the target are too far apart to interact directly (Lamb et al., 2001). Therefore, the flexibility of CCSIII may well be an essential property of the domain in order to shuttle the copper from CCSI into SOD1.

McLoughlin et al. demonstrated that the human CCS and X11α, a neuronal protein related to Alzheimer's disease (AD), interact via their third domain (CCSIII) and second PDZ domain (PDZ2α), respectively (McLoughlin et al., 2001). Consequently, SOD1 cannot acquire copper, and it fails to fulfill its essential physiological role. The authors suggested that X11α might play a role in copper homeostasis. The aim of the work presented here is to determine the type of interaction between the human CCSIII and PDZ2α as a first step towards understanding the molecular details of the inhibition of copper incorporation into SOD1 by X11α.

X11α is a large neuron-specific soluble protein that consists of 5 domains (Okamoto and Sudhof, 1997), involved in various protein–protein interactions. Via its different domains, X11α participates in exocytosis and neurotransmission (Butz et al., 1998). It also prevents the secretion of Aβ, the major component of the senile plaques and fibrils present in the brains of Alzheimer patients (Okamoto and Sudhof, 1997; Biederer et al., 2002; Ho et al., 2002). Interestingly, X11α seems to possess two conflicting functions. While it prevents the development of AD, it exposes neurons to oxidative stress by rendering SOD1 inactive.

PDZ domains are cellular glues. They are present in a large number of proteins, often involved in signal transduction. Their role is to help the formation of protein complexes, usually at the plasma membrane (Fanning and Anderson, 1999; van Ham and Hendriks, 2003). Despite a low sequence similarity among PDZ domains, their structures are remarkably conserved and consist of six β-strands and two α-helices. The classical binding of the carboxy-terminal tail of ligand proteins to PDZ domains occurs in a binding pocket located between βB and αB, creating an

extension to the existing β sheet. This interaction involves a conserved sequence motif (G/Q–L–G–F/I) on the PDZ domain and a conserved arginine N-terminal of this motif that is involved in coordination of the carboxy-terminus of the target via a water molecule. The interacting peptides have traditionally been grouped into four classes on the basis of their C-terminal sequences: Class I involves S/T–x–Φ* sequences (Φ: hydrophobic residue; *: carboxy terminus; x: any residue), Class II involves Φ–x–Φ*, Class III E/D–x–Φ* and Class IV V–x–D/E sequences (Vaccaro and Dente, 2002). It is now well documented that PDZ domains are promiscuous, able to bind C-termini across classes (Palmer et al., 2002; Walma et al., 2002). PDZ domains are also capable of recognizing internal peptide motifs through the very same binding groove (Hillier et al., 1999), such as displayed by the interaction of the second PDZ domain of α1-syntrophin and the C-terminal β-finger of nitrous oxide synthase (NOS). Furthermore, PDZ domains have other interaction surfaces (Feng et al., 2002, 2003; Im et al., 2003), and not only proteins but also phospholipids serve as binding targets (Zimmermann et al., 2002).

Among the 40 residues of the human CCSIII domain, there are two potential binding sites, one at the C-terminus, and the other in the middle of CCSIII. The C-terminal sequence of human CCSIII (AQPPAHL*) only partially fits the class-II consensus sequence, as the penultimate P_{-2} residue of this motif usually comprises a large hydrophobic residue. Alternatively, the residues G^{248}LTIW-EER^{255} could present an internal interaction motif by analogy with the syntrophin–NOS complex.

Using high-resolution NMR spectroscopy we examined the structural basis of the interaction between sequences within CCSIII and PDZ2α. We solved the structure of PDZ2α in solution and explored binding of the two peptides derived from CCSIII mentioned above, as well as several variants of the AQPPAHL peptide.

Material and methods

Protein expression and purification

The sequence coding for residue 745–823 of the human X11α (Swiss-Prot code Q02410) was cloned

by PCR from human brain cDNA into a pET3H expression vector (which provides an N-terminal poly-histidine tag) (Chen and Hai, 1994), with six additional residues (LETMGN) between the His-tag and the PDZ domain. The gene was over-expressed in *E. coli* BL21 (DE3*RP) grown at 28 °C. For isotope labeling, M9 minimal medium was supplemented with $^{15}NH_4Cl$ (0.5 g/l) and either 10% or 100% uniformly labeled ^{13}C-glucose (0.5 or 5 g/l) (CIL, Andover MA). When the OD_{600} of the culture reached 0.6, expression was induced and incubation was continued for 11 h. After centrifugation, the cell pellet was resuspended in 10 ml 20 mM Tris–HCl pH 8.0 and kept at −80 °C until the next step. After thawing, the cells were sonicated in the presence of 1 mM PMSF and 0.1% NP-40 (a non-ionic detergent). The lysate was brought to 0.5 M NaCl prior to centrifugation at 30,000 g for 1 h. The supernatant was loaded onto a Hi-Trap Chelate resin (Pharmacia) saturated with Ni^{2+} and eluted with an imidazole gradient (0–400 mM). The eluted fractions were analysed by SDS-PAGE, and those exhibiting a single band on the gel below 14 kDa were pooled and dialyzed extensively against MilliQ grade water. Precipitates were removed by centrifugation for 10 min at 4500 g. The protein was stored at −80 °C.

NMR spectroscopy

For NMR analysis the purified PDZ2α domain was concentrated to ca. 2.2 mM in 250 μl and brought to 10 mM sodium phosphate buffer pH 6.7. A deuterated sample was obtained by allowing the labile protons for exchange with deuterium and was brought to 10 mM sodium phosphate buffer (in D_2O) pH 6.7. Sequence specific assignments of $^{13}C_{\alpha}$, $^{13}C_{\beta}$, ^{13}CO, ^{15}N, HN and assignments for the side chains (including the carbons and protons, and stereospecific assignment of valine and leucine side chain methyls) were obtained from standard 2-D and 3-D spectra recorded at 290 K. The data were processed using the Azara 2.7 suite of programs (available at www.bio.cam.ac.uk/azara) and analyzed with Ansig for Windows (Helgstrand et al., 2000).

The distance restraints were obtained from 3D ^{15}N-NOESY-HSQC and ^{13}C-NOESY-HSQC spectra, recorded on a Varian Unity Inova 800 MHz spectrometer at 290 K, all with a mixing time of 100 ms. The data were processed with the NMRPipe suite (Delaglio et al., 1995) (http://spin.niddk.nih.gov/bax/software/NMRPipe/) and analysed with CARA (Keller, 2004) (available at http://www.nmr.ch/). The T_1, $T_{1\rho}$ and $\{^1H\}-^{15}N$ NOE experiments were also recorded at 290 K.

Structure calculation

The NOE cross-peak assignments and a consistent tertiary fold were obtained from the automated iterative assignment program CANDID (Herrmann et al., 2002), which works in conjunction with 3-D structure calculations in the program CYANA (Guntert et al., 1997). The calculations consisted of the standard protocol of seven cycles of iterative NOE assignment and structure calculation (Herrmann et al., 2002). In each of the seven cycles the NOEs assigned by CANDID were supplemented by the backbone dihedral angle constraints obtained from analysis of chemical shifts using the program TALOS (Cornilescu et al., 1999).

The final structure calculations with CYANA were started from 100 conformers with random torsion angle values. Simulated annealing with 10,000 time steps per conformer was done using the CYANA torsion angle dynamics algorithm (Guntert et al., 1997). Using the FormatConverter, developed as part of the Collaborative Computing Project for the NMR Community (CCPN) (Fogh et al., 2002), the distance and dihedral angle restraints were converted to the X-PLOR (Brünger, 1992) restraint format. Subsequently the 100 generated structures were refined using a short restrained molecular dynamics simulation in explicit solvent (Linge et al., 2003; Nabuurs et al., 2004) in the program XPLOR-NIH (Schwieters et al., 2003). Of these, the 20 lowest energy structures were selected to form the final ensemble.

The quality of the structure ensemble was judged both by their agreement with the experimental restraints and the quality scores as determined by the structure analysis programs PROCHECK (Laskowski et al., 1993) and WHAT_CHECK (Vriend, 1990). Averages and standard deviations were calculated from the checks of the individual members of the final ensemble. The coordinates have been deposited at the Protein Data Bank, accession code 1Y7N. All figures were made using YASARA (http://www.yasara.org/).

Peptide synthesis

Synthetic peptides were prepared by solid phase technology on a Syro II peptide synthesizer (MultiSyntech, Witten, Germany) at 10 μmol scale as has been described before (Tjabringa et al., 2003). Peptides were dissolved in HOAc/water 1/9 (v/v) and lyophilized overnight. RP-HPLC analysis indicated >90% purity and mass spectrometric analysis (Maldi-Tof, Voyager DE Pro, Perspetive Biosystems, Framingham, USA) confirmed the expected molecular masses.

The peptide sequences were as follows: AQP-PAHL, Ac-AQPPAHL, Ac-AQPPAHL-NH$_2$, Ac-AQPPAHA, Ac-AQPPAAL, Ac-AQPAAHL, and Ac-GLTIWEER-NH$_2$, wherein Ac-indicates an acetylated N-terminus and -NH$_2$ indicates an amidated C-terminus.

Peptide interactions

The interaction studies consisted of titration experiments of the peptides into solutions of PDZ2α. Binding curves were obtained by plotting the chemical shift difference ($\Delta\delta$) of the backbone nitrogen of the most affected residues against the corresponding peptide:protein ratio (R). The dissociation constant (K_D) was derived by individual fitting with the following equation (Kannt et al., 1996) in Origin 7.5 (OriginLab Corporation, Northampton, MA):

$$\Delta\delta = \frac{\Delta\delta_{max}\left(T - \sqrt{T^2 - 4R}\right)}{2}$$

where $T = 1 + R + \frac{K_D([R*A]+B)}{A*B}$, and A is the starting concentration of PDZ2α, B the concentration of the stock solution of peptide, and $\Delta\delta_{max}$ the $\Delta\delta$ at $R \to \infty$.

Results

Solution structure of PDZ2α

The solution structure of the second PDZ domain of X11α (PDZ2α) was solved using high-resolution multi-dimensional heteronuclear NMR. The PDZ2α construct consisted of a six-residue histidine-tag, a non-native engineered linker of six residues (LETMGN), followed by residues 745–

823 of the original X11α sequence (corresponding to residues 12–90 in our numbering – Figure 1a and the Materials and Methods section). Near-complete assignments of ^{1}H, ^{15}N and ^{13}C spectra were obtained using standard procedures and have been deposited in the BMRB data bank (BMB accession number 6113). On the basis of 1690 NOE-derived distance constraints and 95 dihedral restraints (Table 1) an ensemble of NMR structures was calculated using a torsion-angle dynamics protocol. A tube representation and a stereoview of the ensemble (PDB accession code 1Y7N) encompassing residue 7 to 90 are shown in Figure 1b and c, respectively. The first six residues (comprising the His-tag) are not represented because no data were obtained for these residues from the NMR experiments. The ensemble was analyzed using the programs PROCHECK (Laskowski et al., 1993) and WHAT IF (Vriend, 1990), and the structural statistics are reported in Table 1. The pairwise RMSD of the ordered backbone heavy atoms (using residues 14–87) is 0.50 ± 0.10 Å, while the pairwise RMSD of the global backbone heavy atoms is 1.02 ± 0.26 Å, indicating a well-defined ensemble, even for the loop regions. The Ramachandran analysis displays 90.3% of the residues in the most favored regions, and an additional 9.2% in the allowed regions. The average RMS Z-scores values are close to 1, indicating a good covalent geometry of the ensemble.

The ensemble displays a compact fold formed of six β-strands (βA to βF), two α-helices (αA and αB), 3 loops and 4 β-turns (L1–L7), packed in the characteristic PDZ fold. The conserved arginine of the peptide binding motif is situated in loop L1 and the consensus binding motif is between loop L1 and β-strand βB. As expected, the groove for ligand interaction, formed by the second β-strand and the second α-helix, is also present in PDZ2α. Sequence and structural alignment (Figure 1d) show two unique features for the PDZ2α ensemble as compared to other known PDZ domains. First, loop L1 connecting the first and the second β-strand, is longer by two residues (Leu 22 and Arg 23) forming a cap above the binding groove. Although the L1-loop is longer, the position of the consensus binding motif (QLGF) remains structurally unchanged at the border between L1 and the second β-strand, allowing the residues Leu 26 and Gly 27 to form the bulge typical for PDZ domains. Second, the loop L2, situated between
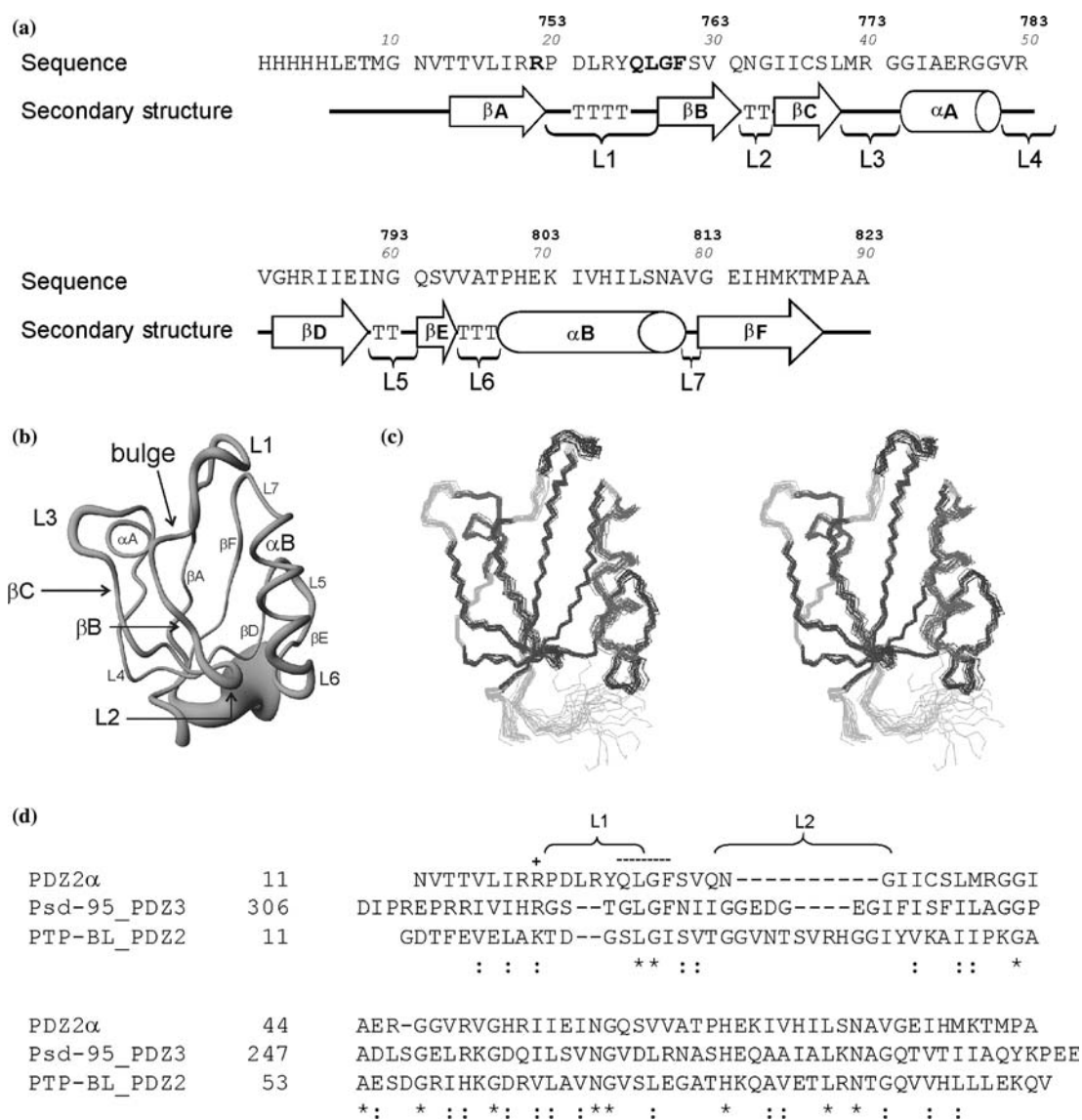
Figure 1. (a) Sequence of the PDZ2α construct. The numbers in normal font correspond to the Swiss-Prot numbering (accession number Q02410). The numbers in italics correspond to the numbering used throughout this paper. The bold residues correspond to the conserved arginine (R19) coordinating the ligand via a water molecule in other PDZ-peptide complexes, and the conserved binding motif (Q25 to F28). The secondary structure elements of PDZ2α are shown below the sequence. T indicates residues in a β-turn. (b) Tube representation of an ensemble of 20 superimposed models of PDZ2α. The diameter of the tube represents the RMSD of the backbone atoms in the ensemble. (c) Stereoview of the PDZ2α ensemble. The α-helices, the β-strands and the β-turns are indicated in dark. (d) Sequence alignment of PDZ2α (PDB accession code 1Y7N) with the third PDZ domain of the synaptic protein Psd-95 (PDB accession code 1BE9 (Doyle et al., 1996)) and the second PDZ domain of the tyrosine phosphatase PTP-BL (PDB accession code 1GM1 (Walma et al., 2002)). The arginine involved in binding the C-terminus of the peptide is indicated with a '+'. The conserved binding motif is indicated with a '- - - -'. Residue similarity is indicated by ':', while residue identity is indicated by '*'.

the second and the third β-strand, consists of only two residues (Asn 32 and Gly 33). It is 6–10 residues shorter when compared to other PDZ domains. However, the positions of the secondary elements with respect to each other are not perturbed (data not shown). The strands βC–βF and the helix αB align well with their homologues in the third PDZ domain of Psd-95 (PDB accession code 1BE9 (Doyle et al., 1996)) and the second PDZ domain of PTP-BL (PDB accession code

Table 1. Structural statistics for the ensemble of the 20 best models of the PDZ2α[a]

A. Restraint information	
Distance restraints (intra-residual/ sequential/medium/long)	1690 (313/442/324/611)
Hydrogen bonding restraints	–
Dihedral angle restraints (phi/psi)	95 (48/47)
Structural uncertainty (bits/atom^2, $I_{total}/H_{structure|R}$)[b]	1.911/4.359
Information distribution (%, dihedral/intra-residual/ sequential/medium/long)[b]	1.1/0.2/0.7/15.0/83.0
B. Average RMS deviation from experimental restraints	
Distance restraints (Å)	0.021 ± 0.001
Dihedral angle restraints (deg.)	0.32 ± 0.08
C. Pairwise Cartesian RMS deviation (Å)	
Global backbone heavy atoms	1.02 ± 0.26
Global all heavy atoms	1.65 ± 0.22
Ordered[c] backbone heavy atoms	0.50 ± 0.10
Ordered[c] all heavy atoms	1.22 ± 0.13
D. Ramachandran quality parameters (%)[d]	
Residues in favored regions	90.3
Residues in allowed regions	9.2
Residues in additionally allowed regions	0.4
Residues in disallowed regions	0.1
E. Average RMS deviation from current reliable structures (RMS Z-scores, null deviation = 1)[e]	
Bond lengths	0.97
Bond angles	0.83
Omega angle restraints	0.60
Side-chain planarity	0.98
Improper dihedral distribution	0.78
Inside/outside distribution	0.98
F. Average deviation from current liable structures (Z-scores, null deviation = 0)[e]	
1st generation packing quality	−1.0
2nd generation packing quality	0.3
Ramachandran plot appearance	−2.5
Chi-1 / chi-2 rotamer normality	−1.3
Backbone conformation	−1.9

[a]PDB accession code: 1Y7N.
[b]Values calculated using QUEEN (Nabuurs et al., 2004).
[c]Residues involved in secondary structure: 14–87.
[d]Values based on PROCHECK (Laskowski et al., 1993) output.
[e]Values based on WHATCHECK (Laskowski et al., 1993) output.

1GM1 (Walma et al., 2002)). Only the helix αA does not align well with its homologue on the other two PDZ domains.

Dynamics

^{15}N relaxation measurements ($\{^1H\}-^{15}N$ NOE, ^{15}N-R_1 and ^{15}N-$R_{1\rho}$) were recorded on PDZ2α. The resulting data were used to calculate the overall tumbling rate (τ_c), the internal correlation time (τ_e) and the order parameters (S^2) using the model-free approach (Lipari and Szabo, 1982a, 1982b) (see Figure S1 in Supplemental Data) as implemented in the program Modelfree 4.01 (Mandel et al., 1995). Prolines 20, 67 and 88, valine 49 and isoleucines 58 and 71 were not taken into account (because of spectral overlap for the latter three). The overall tumbling rate of PDZ2α is described by an isotropic model with an average global correlation time of 7.1 ± 0.8 ns, which is a typical value for such a small, folded protein at 290 K. The local motion of 38 residues is described by a model incorporating only the S^2 parameter, 31 residues by a model requiring both S^2 and τ_e parameters, and 3 residues by a model with motions on the pico- and sub-nanosecond time scales as described by the S^2, S^2_1 and τ_e parameters. Four residues (Arg 19, Val 64, Ala 65 and Thr 66) require a model incorporating chemical exchange, as is also evident from their increased $R_{1\rho}$ relaxation rates. Interestingly, Arg 19 is the conserved residue involved in coordinating a bridging water molecule in the peptide binding pocket. The latter three residues are located in the loop L6, connecting βE and αB. Flexible residues, displaying more pronounced motion on the ps-ns timescale are found at the N- and C-termini of PDZ2α and in the proximal part of βA, the loops L1, L3, L7 and part of βF.

Peptide binding to PDZ2α

To test the interactions between PDZ2α and CCSIII, the two potential interaction motifs of CCSIII were examined. Peptide 1, present in the middle of CCSIII, consisted of the sequence Ac-GLTIWEER-NH$_2$, where Ac- and -NH$_2$ correspond to the neutralizing acetyl- and amide-groups, respectively. Peptide 2 corresponds to the last seven residues at the C-terminus of CCSIII with a neutralized N-terminal alanine (Ac-AQPPAHL). Each peptide was titrated into a solution of 1 mM of PDZ2α, and the binding was followed by NMR. At each titration point, a 2-D ^1H,^{15}N-HSQC spectrum of ^{15}N-labeled PDZ2α was recorded.

Addition of Ac-GLTIWEER-NH$_2$ to PDZ2α only resulted in very small chemical shift perturbations in the HSQC spectrum at high peptide to protein ratio (data not shown), from which we conclude that no specific interaction occurred. In contrast, many resonances in the NMR spectrum PDZ2α exhibit a clear shift perturbation upon addition of the Ac-AQP-PAHL peptide (Figure 2a), indicating a specific interaction between the peptide and the protein. Resonances with small perturbations remain visible during the entire titration, while others are broadened at the same peptide:protein ratio due to an intermediate exchange regime. At 20:1 peptide:protein ratio all resonances, with exception of Leu 26, reappear, indicating near-complete saturation of the protein with peptide. These results suggest a dissociation rate constant on the order of 10^3 s^{-1}.

From the chemical shift perturbations (Figure 2b) the dissociation constant (K_D) of PDZ2α for Ac-AQPPAHL was determined to be 91 ± 2 μM. This value is the average of the K_D obtained for each residue (Glu 57, Lys 70, Val 79) individually. It is in the range of other NMR determined dissociation constants of PDZ-ligands complexes, with values in the low μM to several hundreds μM range (Harris et al., 2001; van den Berk et al., 2004).

Chemical shift perturbations have been mapped onto the backbone of PDZ2α (Figure 2c and Table S1 in Supplemental Data). Many of the residues most affected by the presence of Ac-AQPPAHL are located along the second β-strand (βB) with Gly 27 and Phe 28 comprising the canonical binding motif. As mentioned above, the extensive broadening of Leu 26 precludes determination of the perturbation size, but it is easily rationalized by the binding interaction.

Importance of the residues of Ac-AQPPAHL in binding

To establish the relative importance of the individual residues of the Ac-AQPPAHL peptide for binding to PDZ2α, titrations were performed with several peptide variants.

Interaction of PDZ domains with their C-terminal targets has been reported to involve the last four to six residues of the peptide (Fanning and Anderson, 1999), although interactions down to

residue P$_{-8}$ have also been postulated (Birrane et al., 2003; Cai et al., 2002). Here, P$_0$ (denoting the C-terminal residue), P$_{-1}$, and P$_{-3}$ residues were changed into an alanine. Also, the influence of the N- and C-termini of the peptide on the affinity was studied. The binding affinities of PDZ2α for each peptide were derived from NMR titration experiments as described above, and are summarized in Table 2. The largest changes in affinity are observed when the last residue (P$_0$) is altered. When the carboxy-group is neutralized by the presence of an amide group, binding is completely abolished. When the P$_0$ residue is changed from a leucine to an alanine, the affinity decreases 160 fold. The presence of a positive charge at the P$_{-6}$ residue of the peptide decreases the affinity by a factor 3. When the proline P$_{-3}$ is changed into an alanine, the affinity remains unchanged. Interestingly, when the histidine is changed into an alanine the affinity increases by a factor of two.

The titrations also reveal that the observed effects for specific residues of PDZ2α are dependent upon the specific peptide variant. We quantified these differences in chemical shift perturbation and mapped the result onto the structure of PDZ2α (Figure 3). The residues of PDZ2α that show a different chemical shift perturbation pattern between the native peptide (Ac-AQPPAHL) and the P$_0$ alanine-variant are the conserved Arg19, Gly 27 and Phe 28 of the binding motif, residue Val 30, and residues His 73, Ile 74, Leu 75, Ser 76 and Asn 77 of the helix αB. The only residue that is significantly affected by the P$_{-1}$-variant is Gly 27, although an effect on Leu 26 cannot be ruled out. Three residues, (Asn 32, Gly 33, and Glu 69, located at the top of βB and the bottom of αB) sense the change at the P$_{-3}$ position.

Discussion

Although the sequence conservation of different PDZ domains is rather low, the PDZ fold is conserved, with six β-strands and two α-helices which superimpose well onto known PDZ domains.

A structural model of PDZ2α (called PDZ2αM) had been generated by sequence alignment with the third PDZ domain of Psd-95 (PDB accession code 1BE9 (Doyle et al., 1996)), using the programs ClustalW and SwissModel (available at http://www.ch.embnet.org/software/
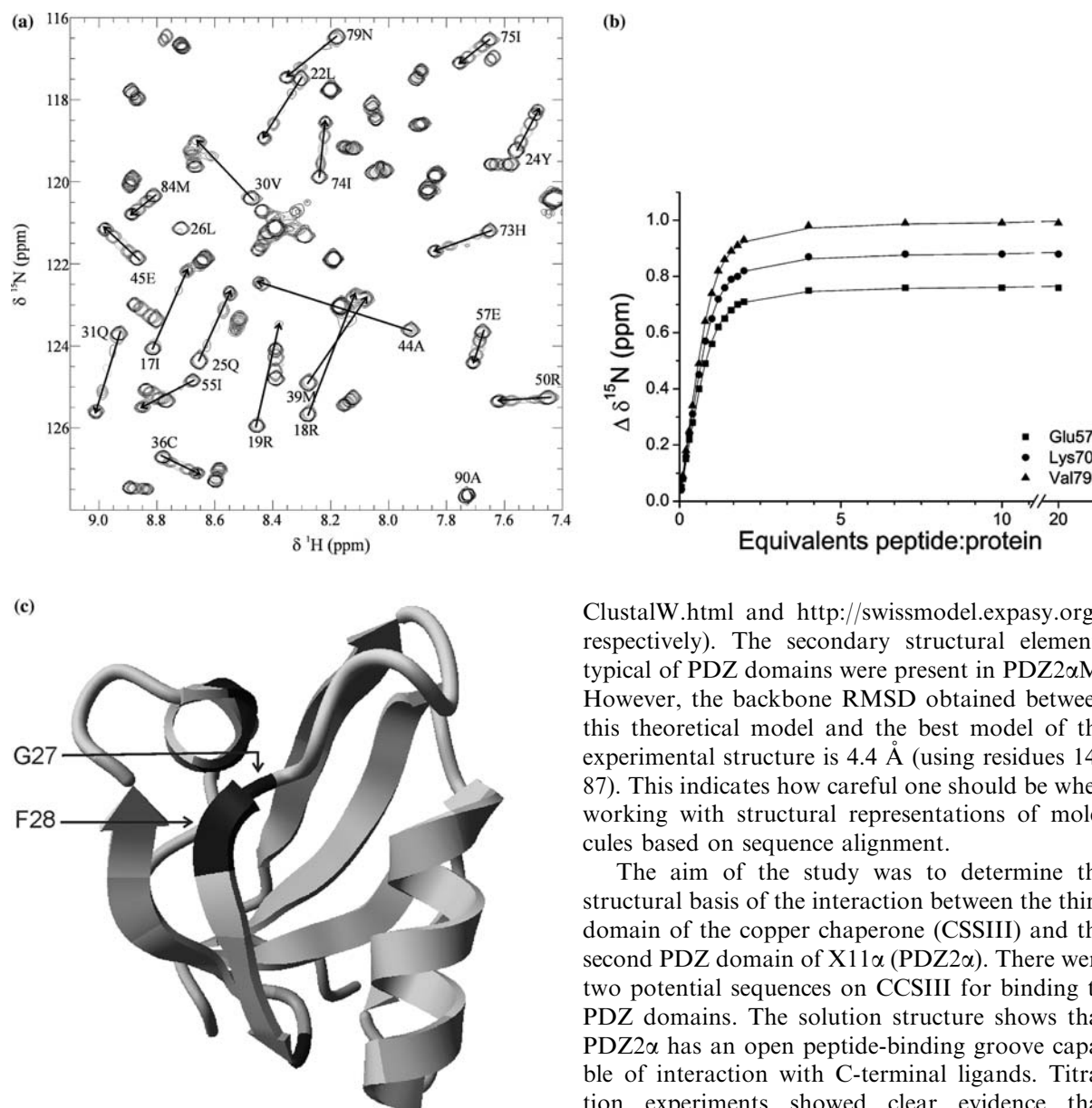
Figure 2. (a) Chemical shift perturbations of PDZ2α upon addition of Ac-AQPPAHL. The overlaid ^{1}H,^{15}N-HSQC spectra correspond to the following peptide:protein ratios: 0.0, 0.05, 0.3, 0.6, 1.0, 4.0, and 20.0. The arrows indicate the direction of the chemical shift perturbation. (b) Binding curves for Ac-AQPPAHL to PDZ2α. The chemical shift perturbations of the ^{15}N amide nuclei of Glu 57, Lys 70 and Val 79 are plotted against the peptide:protein ratio and have been fitted individually with a 1:1 binding model (Kannt et al., 1996), yielding a K_D of 91 ± 2 μM. (c) Mapping of the effect of Ac-AQPPAHL on PDZ2α. The darker colours correspond to the largest effects.

ClustalW.html and http://swissmodel.expasy.org/, respectively). The secondary structural elements typical of PDZ domains were present in PDZ2αM. However, the backbone RMSD obtained between this theoretical model and the best model of the experimental structure is 4.4 Å (using residues 14–87). This indicates how careful one should be when working with structural representations of molecules based on sequence alignment.

The aim of the study was to determine the structural basis of the interaction between the third domain of the copper chaperone (CSSIII) and the second PDZ domain of X11α (PDZ2α). There were two potential sequences on CCSIII for binding to PDZ domains. The solution structure shows that PDZ2α has an open peptide-binding groove capable of interaction with C-terminal ligands. Titration experiments showed clear evidence that PDZ2α specifically binds a peptide corresponding to the six C-terminal residues of CCS, and not to one that represents an internal site of CCSIII. This interaction suggests that X11α could inhibit the activity of CCS by decreasing the flexibility of the CCSIII domain.

The contribution of the residues in the CCSIII peptide to the binding could be dissected using peptide variants. The loss of affinity resulting from the Leu to Ala mutation of the C-terminal residue

Table 2. Summary of the dissociation constants of PDZ2α for the native peptide (Ac-AQPPAHL) and several variants

Peptide	K_D (μM)	Relative affinity
Ac-AQPPAHL	91 ± 2	1
Ac-AQPPAHL-**NH₂**	> 55,000	< 0.0016
Ac-AQPPAH**A**	14,300 ± 200	0.006
Ac-AQPPA**A**L	47 ± 4	2
Ac-AQP**A**AHL	98 ± 2	1
H₃N⁺−AQPPAHL	300 ± 8	0.3

The modified residues are in bold. Ac- and -NH₂ represent an acetylated N-terminus and C-terminus with an amide group, respectively.

or the removal of the terminal carboxy-group clearly indicates that the peptide binds in a canonical fashion between βB strand and αB helix, despite its non-canonical sequence. By quantifying differential chemical shift effects upon changes of the CCSIII peptide, it is possible to probe specific interactions between PDZ2α residues and residues in the peptide. These experimental data are in agreement with a structure-based model of the PDZ2α-CCSIII peptide complex (Figure 3) constructed using the complex of Psd-95 and its ligand as a template. Residues sensitive to the P$_0$ alanine-variant (Figure 3, shown in red) line the top of the
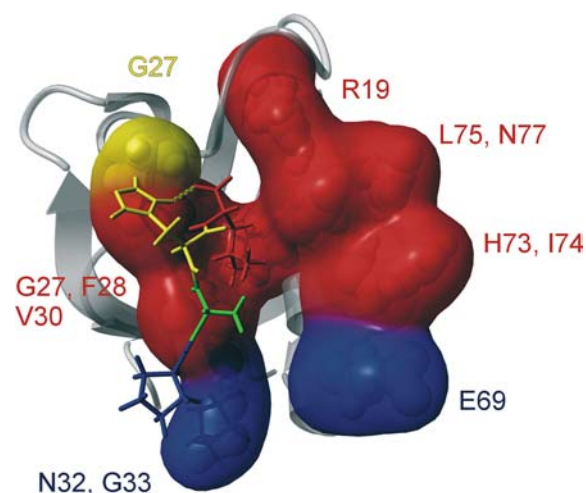

Figure 3. Model of the last four residues (PAHL) of CCSIII in the PDZ2α binding groove. The effects observed upon binding of the P$_0$, P$_{-1}$ and P$_{-3}$-variants are represented in red, yellow and blue, respectively. The model has been obtained by structural alignment of PDZ2α and PAHL with the third PDZ domain of the synaptic protein Psd-95 bound to its peptide ligand (PDB accession code 1BE9 (Doyle et al., 1996)).

PDZ2α binding groove and illustrate its importance for binding. The side chain of the P$_0$ leucine is highly buried inside the binding groove, pointing towards the residues present in helix αB. The P$_{-1}$-variant showed a surprising increase in affinity. The chemical shift analysis revealed that Gly 27 (in yellow in Figure 3) was the only residue significantly affected by this mutation. The imidazole ring of the histidine P$_{-1}$ is oriented toward that Gly 27 of PDZ2α. The increased affinity observed for the P$_{-1}$-variant can be rationalized by the presence of a hydrogen bond between the imidazole ring of the P$_{-1}$ histidine and the carboxy-terminal group of the peptide. When P$_{-1}$ histidine is changed into an alanine, this hydrogen bond can no longer be formed, and the carboxylic group becomes more available for binding to the protein. Residues at the P$_{-1}$ position have traditionally been classified as unimportant for PDZ-target binding (Doyle et al., 1996), but more recent reports have illustrated their importance (Kang et al., 2003; Walma, 2004). In these more recent views, the PDZ domains contain multiple, sometimes mutually exclusive pockets, through which interactions are formed, with the P$_{-1}$ residue potentially providing an essential discriminatory role (Walma, 2004). The P$_{-2}$ residue is traditionally a crucial determinant for either class I or class II peptides. It usually is a large hydrophobic residue pointing to the top of the helix αB. In the PDZ2α-CSSIII peptide complex, the P$_{-2}$ residue is an alanine. Its small hydrophobic side chain is well suited for an orientation inside the protein, towards the side chain of Val 72, with which it probably makes stable hydrophobic contact. Finally, the P$_{-3}$ residue is located in the proximity of Asn 32 and Gly 33, at the C-terminus of βB, and Glu 69 at the N-terminus of αB, but it is not likely to be involved in binding as its mutation does not affect affinity.

218

References

Biederer, T., Cao, X.W., Sudhof, T.C. and Liu, X.R. (2002) *J. Neurosci.* **22**, 7340–7351.

Birrane, G., Chung, J. and Ladias, J.A.A. (2003) *J. Biol. Chem.* **278**, 1399–1402.

Brünger, A. (1992) *X-PLOR version 3.1. A system for X-ray crystallography and NMR*, Yale University Press, New Haven, CT.

Butz, S., Okamoto, M. and Sudhof, T.C. (1998) *Cell* **94**, 773–782.

Cai, C., Coleman, S.K., Niemi, K. and Keinanen, K. (2002) *J. Biol. Chem.* **277**, 31484–31490.

Chen, B.P.C. and Hai, T.W. (1994) *Gene* **139**, 73–75.

Cornilescu, G., Delaglio, F. and Bax, A. (1999) *J. Biomol. NMR* **13**, 289–302.

Culotta, V.C., Klomp, L.W.J., Strain, J., Casareno, R.L.B., Krems, B. and Gitlin, J.D. (1997) *J. Biol. Chem.* **272**, 23469–23472.

Delaglio, F., Grzesiek, S., Vuister, G.W., Zhu, G., Pfeifer, J. and Bax, A. (1995) *J. Biomol. NMR* **6**, 277–293.

Doyle, D.A., Lee, A., Lewis, J., Kim, E., Sheng, M. and MacKinnon, R. (1996) *Cell* **85**, 1067–1076.

Falconi, M., Iovino, M. and Desideri, A. (1999) *Structure* **7**, 903–908.

Fanning, A.S. and Anderson, J.M. (1999) *J. Clin. Invest.* **103**, 767–772.

Feng, W., Fan, J.S., Jiang, M., Shi, Y.W. and Zhang, M. (2002) *J. Biol. Chem.* **277**, 41140–41146.

Feng, W., Shi, Y.W., Li, M. and Zhang, M.J. (2003) *Nat. Struct. Biol.* **10**, 972–978.

Fogh, R., Ionides, J., Ulrich, E., Boucher, W., Vranken, W., Linge, J.P., Rieping, W., Bhat, T.N., Westbrook, J., Henrick, K., Gilliland, G., Berman, H., Thornton, J., Nilges, M., Markley, J. and Laue, E. (2002) *Nat. Struct. Biol.* **9**, 416–418.

Guntert, P., Mumenthaler, C. and Wuthrich, K. (1997) *J. Mol. Biol.* **273**, 283–298.

Harris, B.Z., Hillier, B.J. and Lim, W.A. (2001) *Biochemistry (Mosc)*. **40**, 5921–5930.

Harrison, M.D., Jones, C.E. and Dameron, C.T. (1999) *J. Biol. Inorg. Chem.* **4**, 145–153.

Helgstrand, M., Kraulis, P., Allard, P. and Hard, T. (2000) *J. Biomol. NMR* **18**, 329–336.

Herrmann, T., Guntert, P. and Wuthrich, K. (2002) *J. Mol. Biol.* **319**, 209–227.

Hillier, B.J., Christopherson, K.S., Prehoda, K.E., Bredt, D.S. and Lim, W.A. (1999) *Science* **284**, 812–815.

Ho, C.S., Marinescu, V., Steinhilb, M.L., Gaut, J.R., Turner, R.S. and Stuenkel, E.L. (2002) *J. Biol. Chem.* **277**, 27021–27028.

Im, Y.J., Lee, J.H., Park, S.H., Park, S.J., Rho, S.H., Kang, G.B., Kim, E. and Eom, S.H. (2003) *J. Biol. Chem.* **278**, 48099–48104.

Kang, B.S., Cooper, D.R., Devedjiev, Y., Derewenda, U. and Derewenda, Z.S. (2003) *Structure* **11**, 845–853.

Kannt, A., Young, S. and Bendall, D.S. (1996) *Biochim. Biophys. Acta* **1277**, 115–126.

Keller, R. (2004) *The Computer Aided Resonance Assignment Tutorial* CANTINA, Verlag.

Lamb, A.L., Torres, A.S., O'Halloran, T.V. and Rosenzweig, A.C. (2001) *Nat. Struct. Biol.* **8**, 751–755.

Lamb, A.L., Wernimont, A.K., Pufahl, R.A., Culotta, V.C., O'Halloran, T.V. and Rosenzweig, A.C. (1999) *Nat. Struct. Biol.* **6**, 724–729.

Laskowski, R.A., Macarthur, M.W., Moss, D.S. and Thornton, J.M. (1993) *Journal of Applied Crystallography* **26**, 283–291.

Linge, J.P., Williams, M.A., Spronk, C., Bonvin, A. and Nilges, M. (2003) *Prot.-Struc. Func. Gen.* **50**, 496–506.

Lipari, G. and Szabo, A. (1982a) *J. Am. Chem. Soc.* **104**, 4546–4559.

Lipari, G. and Szabo, A. (1982b) *J. Am. Chem. Soc.* **104**, 4559–4570.

Mandel, A.M., Akke, M. and Palmer, A.G. (1995) *J. Mol. Biol.* **246**, 144–163.

McLoughlin, D.M., Standen, C.L., Lau, K.F., Ackerley, S., Bartnikas, T.P., Gitlin, J.D. and Miller, C.C.J. (2001) *J. Biol. Chem.* **276**, 9303–9307.

Nabuurs, S.B., Nederveen, A.J., Vranken, W., Doreleijers, J.F., Bonvin, A., Vuister, G.W., Vriend, G. and Spronk, C. (2004) *Prot.-Struc. Func. Bioinformatics* **55**, 483–486.

O'Halloran, T.V. and Culotta, V.C. (2000) *J. Biol. Chem.* **275**, 25057–25060.

Okamoto, M. and Sudhof, T.C. (1997) *J. Biol. Chem.* **272**, 31459–31464.

Palmer, A., Zimmer, M., Erdmann, K.S., Eulenburg, V., Porthin, A., Heumann, R., Deutsch, U. and Klein, R. (2002) *Mol. Cell* **9**, 725–737.

Pena, M.M.O., Lee, J. and Thiele, D.J. (1999) *J. Nutr.* **129**, 1251–1260.

Rae, T.D., Schmidt, P.J., Pufahl, R.A., Culotta, V.C. and O'Halloran, T.V. (1999) *Science* **284**, 805–808.

Rosenzweig, A.C. and O'Halloran, T.V. (2000) *Curr. Opin. Chem. Biol.* **4**, 140–147.

Schwieters, C.D., Kuszewski, J.J., Tjandra, N. and Clore, G.M. (2003) *J. Magn. Reson.* **160**, 65–73.

Tjabringa, G.S., Aarbiou, J., Ninaber, D.K., Drijfhout, J.W., Sorensen, O.E., Borregaard, N., Rabe, K.F. and Hiemstra, P.S. (2003) *J. Immunol.* **171**, 6690–6696.

Vaccaro, P. and Dente, L. (2002) *FEBS Lett.* **512**, 345–346.

van den Berk, L.C. , van Ham, M.A. , te Lindert, M.M., Walma, T., Aelen, J., Vuister, G.W. and Hendriks, W.J. (2004) *Mol. Biol. Rep.* **31**, 203–215.

van Ham, M. and Hendriks, W. (2003) *Mol. Biol. Rep.* **30**, 69–82.

Vriend, G. (1990) *J. Mol. Graph.* **8**, 52–56.

Walma, T. (2004) *The second PDZ domain of PTP-BL*, Ph.D. thesis, Radboud University of Nijmegen.

Walma, T., Spronk, C.A.E.M., Tessari, M., Aelen, J., Schepens, J., Hendriks, W. and Vuister, G.W. (2002) *J. Mol. Biol.* **316**, 1101–1110.

Zimmermann, P., Meerschaert, K., Reekmans, G., Leenaerts, I., Small, J.V., Vandekerckhove, J., David, G. and Gettemans, J. (2002) *Mol. Cell* **9**, 1215–1225.